Incident Power and Relative Phase Distribution Mapping in Reconfigurable Intelligent Surfaces Using Energy Harvesting

Md Abu Saleh Tajin, *Student Member, IEEE*, Kyei Anim, and Kapil R. Dandekar, *Senior Member, IEEE*

***Abstract*— One of the major challenges of reconfigurable intelligent surfaces (RISs) is the large state-selection search space that demands real-time programmability and fast processing. The knowledge of incident power and relative phase distribution across an RIS can potentially simplify the state-selection process. Herein, we present a novel method of obtaining incident power and relative phase distribution using energy harvesting circuits (rectifiers) that can be integrated into the RIS. Four versions of the energy harvesting circuit are proposed that offer great control over the sensitivity of the system. The sensitivity of the proposed rectifier circuit is −42 dBm for direct rectification. The inclusion of direct current (dc) bias and radio frequency (RF) amplifiers greatly increases the sensitivity of the rectifiers. The received power and phase distribution across the unit dipoles of RIS are simulated to demonstrate the potential of the proposed method. Experiments are performed in an indoor environment at 2.1 GHz. Experimental results show that the proposed energy harvesting method can successfully predict the received power distribution for angular and perpendicular incidence of the incident radio waves.**

***Index Terms*— 6G, energy harvesting, reconfigurable intelligent surface (RIS), rectifier, RIS state selection.**

I. Introduction

RECONFIGURABLE intelligent surfaces (RISs) are an exciting new technology for next-generation wireless networks. While the electromagnetic propagation channel is generally considered to be an immutable black box, RIS provides the ability to modify the wireless channel in a manner that is beneficial to the overlying wireless system. The working principle of an RIS is analogous to 2-D phased array antennas. By selectively activating unit cells, the reflected signals (from RIS unit cells) add up constructively to a certain direction, enabling beam-steering capability. In an RIS, the power and phase distribution of the reflected signals (across the surface) are unknown to the controller. As a result, the RIS state selection can be considered a problem of driving a 2-D phased array without any information about the power and phase of the input signals at the array elements. Our work aims to offer a novel and pragmatic approach to obtaining the power and relative phase distribution throughout the RIS to better inform future state-selection algorithms.

We are proposing a new method of extracting incident power and relative phase distribution in an RIS by forming energy harvesting rectennas using RIS elements and rectifier circuits. Rectennas are simple and passive circuits consisting of a radio frequency (RF) matching network and a rectifier block with diodes, capacitors, and resistors in general. The incorporation of energy harvesting components/rectifiers in RIS is a relatively new and unexplored research domain. Clerckx et al. [1] proposed the use of rectennas with RIS for wireless information and power transfer applications.

We propose the combination of preselected RIS unit cells with RF–direct current (dc) conversion circuits to form rectennas for the estimation of incident power and relative phase distribution. We have developed four versions of the rectifier circuit, offering strong control of the spatial operating range and complexity of the circuit. The radiated power level of many mobile and IoT devices are low due to energy constraints and external restrictions. As a result, the power of the radio wave eventually reaching the RIS can be insufficient for some rectifier circuits. Thus, we propose dc bias (or dc insertion alongside RF into the rectifier circuit) to activate the rectifier circuit with low RF power levels. This results in a reduction of the input power threshold and enhancement in the sensitivity of the rectifier. To our knowledge, we are the first to propose this type of prebias option in energy harvesting rectifiers. Additionally, the availability of surface-mount and compact RF amplifiers makes them suitable for insertion into the RF–dc conversion circuits. The combination of dc bias and RF amplifier further increases the rectifier sensitivity.

RISs are mostly passive. As a result, it is difficult to acquire channel state information (CSI) from the RIS. Although rapid state selection is a fundamental requirement for the effective deployment of RIS, it is still a challenging and lengthy process. Optimization [2], machine learning (ML), and digital twining [3] have been proposed for RIS state selection. However, they require significant computational effort and environment-specific training. To realize the full benefit of RIS, it is important to have knowledge of the power and phase distribution of incident radio waves across the RIS. Although this information can be collected by deploying radios across the RIS [4], the overall system will be complicated and expensive, requiring synchronization and control. Our proposed method is flexible and inexpensive. The harvested energy map (or received power distribution) is readily available to the RIS controller which can be used for state selection based on the requirements.

Manuscript received 20 May 2022; revised 17 March 2023; accepted 10 April 2023. Date of publication 18 April 2023; date of current version 7 July 2023. This work was supported by the National Science Foundation under Grant CNS-1816387. *(Md Abu Saleh Tajin and Kyei Anim contributed equally to this work.) (Corresponding author: Kapil R. Dandekar.)*

The authors are with the Department of Electrical and Computer Engineering, Drexel University, Philadelphia, PA 19104 USA (e-mail: mt3223@drexel.edu; ak4259@drexel.edu; dandekar@drexel.edu).

Color versions of one or more figures in this article are available at https://doi.org/10.1109/TAP.2023.3266844.

Digital Object Identifier 10.1109/TAP.2023.3266844

To the best of our knowledge, we are the first to propose the integration of energy harvesting circuits with RIS in order to sense incident power distribution and predict relative phase distribution.

II. Related Work

Although RIS research on the realization of hardware platforms for wireless communications is still in its infancy, a few relevant research works in the open literature can be found. For example, Arun and Balakrishnan [2] propose RFocus that behaves, conceptually, as a programmable "mirror" and as a programmable "lens". The RFocus prototype comprises 3720 passive reflecting elements of size $\lambda/4 \times \lambda/10$ arranged on a 6 m^2 surface, where λ denotes the wavelength. The elements are connected columnwise by voltage-controlled RF switches, which can be in one of two states ("ON" or "OFF" state) to determine whether or not two adjacent elements are connected to form a half dipole antenna. Kashyap et al. [5] use a randomized delay phase along with the antenna and the switch as a unit cell to implement a 1-bit 30×30 randomized RIS aimed at 222.5 GHz within the THz band. In the design, the delays are implemented using microstrip lines. Kamoda et al. [6] propose a microstrip patch element with a single-bit phase shifter to design a 60×60 RIS at 60 GHz. A p-i-n diode is used to make the phase shifters electronically controllable. Tan et al. [7] loaded a microstrip patch with an electronically controlled relay switch to prototype a 60 GHz RIS board. The patch turns on and becomes a resonant reflector when the switch is open to isolate it from the ground plane. Conversely, when the switch is closed, the patch is shorted by the ground plane and transitions to the "OFF"-state that has the minimum reflection. In [8], [9], and [10], the authors propose RIS prototypes based on metasurface or metamaterial unit cells. Each unit cell includes a varactor or p-i-n diode on the top layer controlled by the external bias voltage through the dc biasing lines located on the bottom layer. The middle layer contains the ground plane structure to enhance the reflection of the impinging waves on the RIS. The vias are thus utilized to connect the middle-layer ground plane to the top-layer metal units.

This article proposes a new technique for EM design of RIS that leverages power-harvesting rectifier circuits sparsely distributed throughout the surface in addition to controllable reflectors such as those found in previous RIS designs. This design approach enables sensing capabilities that limit the state-selection search space by learning the incident power and phase of signals impinging on different parts of the surface to help determine the unit cells that would have the most impact on the metrics being optimized by the overlying RIS controller. Furthermore, the proposed RIS not only function, conceptually, as a "mirror" to reflect the impinging signals but also function as a programmable "lens" when the communicating nodes are on the opposite sides of the surface. Thus, our proposed RIS design does not require any ground plane, unlike many RIS prototypes in the literature, and each unit cell contains a voltage-controlled RF switch which allows for microwave transparency in the "OFF" state.

The operation of the RIS generally has two phases: 1) control and programming phase (to configure the RIS based on channel information) and 2) normal operation phase (when RIS has already been configured and ready to assist the transmission). Similar to the aforementioned prototypes, the RIS configuration optimization in the control and programming phase for application to wireless communications has vastly relied on analytics-based solutions (i.e., information theory, mathematical models, signal processing, and optimization algorithms). Although very successful, the traditional analytics-based approach to optimally configuring a very large array of RIS elements remains a challenge given the nearly passive nature of the RIS (i.e., passively reflecting the incident waves) and the increased complexity of communication networks.

Due to recent advances in ML technology, especially in deep learning (DL), some researchers have combined model-based and data-driven approaches to overcome the inherent limitations. Huang et al. [12] present a deep neural network (DNN) model that utilizes the sampled channel knowledge from active RIS elements as input to train the proposed DNN model offline to predict the optimal reflection beamforming matrix of the RIS in a supervised learning setting. Liaskos et al. [13] propose a neural-network-based method to configure the behavior of active RIS elements. The wireless channel is modeled as a custom, interpretable, back-propagating neural network, where the RIS elements act as nodes and their cross-interactions as links. Thus, the neural network learns how to configure the RISs to improve communication performance once the training phase is complete.

Although ML and artificial intelligence (AI) may constitute efficient methods for optimally configuring the most appropriate operation of the RIS in the state-selection process, the training models in "big" data ML are both computationally and memory intensive. On the other hand, equipping the RIS surface with rectifiers as proposed in this article to support the RIS state-selection process automatically reduces the computational burden by limiting the search space based on the knowledge of the power and phase of impinging waves.

III. RIS Simulation

A. RIS Design

The RIS design (Fig. 1) is inspired by RFocus [2]. We simulate and fabricate an 8×11 RIS (Fig. 1). Each rectangular tile measures 21×8.4 mm. The tile length is approximately $\lambda_\epsilon/4$, where λ_ϵ is the effective wavelength due to the dielectric polyethylene substrate (relative permittivity, $\epsilon = 2.25$ in HFSS). Two adjacent RIS tiles form a dipole when they are connected (columnwise) by an RF switch. When all the RF switches are turned off, the RIS allows RF wave propagation and blocks when the switches are turned on. Selective activation of the RF switches converts the RIS structure into a phased array antenna where the input signal on each array element is the reflected signal. We place a lumped port between the fourth and fifth rows on the seventh column (Fig. 1). Each unit dipole is resonant at 2.1 GHz (Fig. 2). Fig. 3 shows the 2-D radiation pattern of a unit dipole around the yz plane (azimuth in the experimental area). While a dipole in free space shows an omnidirectional radiation pattern, the RIS dipole pattern is heavily influenced by the parasitic presence of other unit cells around it.

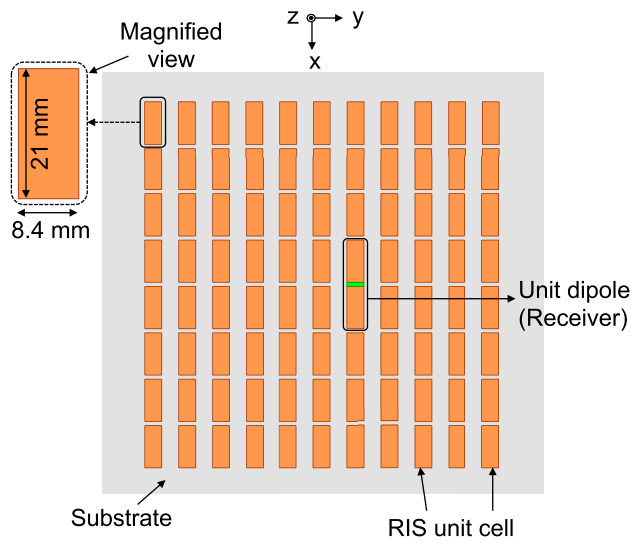

Fig. 1. HFSS simulation model of the RIS.

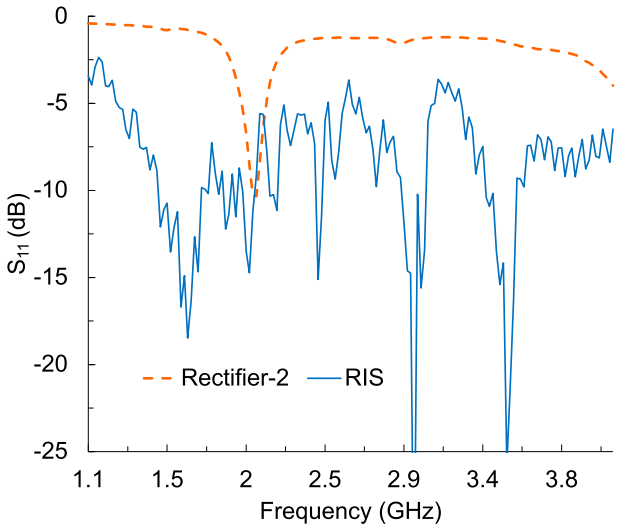

Fig. 2. S_{11} versus frequency plot of the rectifier prototypes and the RIS unit cell dipole.

B. Angular Incidence Simulation

1) One-Dimensional Arrangement: We simulated (2.1 GHz) an RIS with 158 columns of unit cells along the x-axis (Fig. 4) in MATLAB. The unit cell orientation and arrangement are identical to the RIS in Fig. 1. A transmitter (Tx) is 3 m away from the first receiver (Rx1) along the negative x-direction. We assumed that each receiver element (Rx1, Rx2, Rx3, . . . , Rx158) demonstrates the 2-D radiation pattern of the RIS unit cell shown in Fig. 3. We observe the presence of two nulls (low gain zones) in the radiation pattern on both sides of the RIS. Although an ideal dipole would have an omnidirectional radiation pattern around its axis, the surrounding unit cells distort the radiation pattern of the unit dipoles in RIS.

The power received by a receiver unit is calculated using the path loss equation

$$P_{\text{rx}} = P_{\text{in}} + G_{\text{tx}}(\theta) + G_{\text{rx}}(\theta) + 20\ log_{10}\left(\frac{\lambda}{4\pi r}\right) \quad (1)$$

$$r = \sqrt{(3+x)^2 + z^2} \quad (2)$$

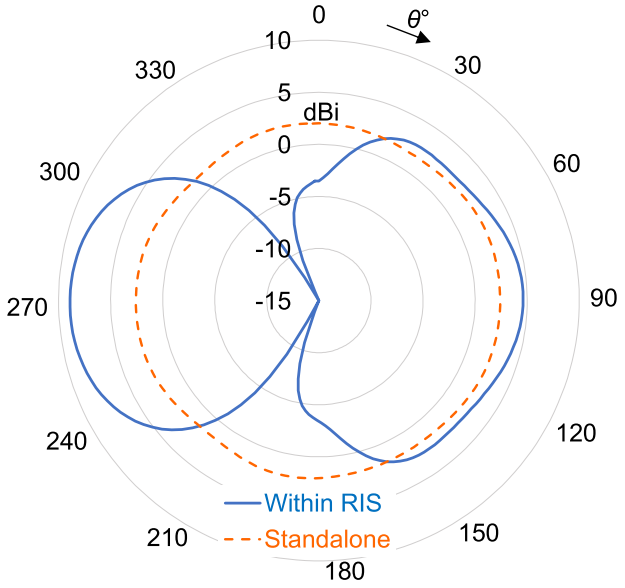

Fig. 3. Radiation pattern of the RIS unit cell. The standalone omnidirectional pattern becomes distorted when the unit dipole is within an RIS.

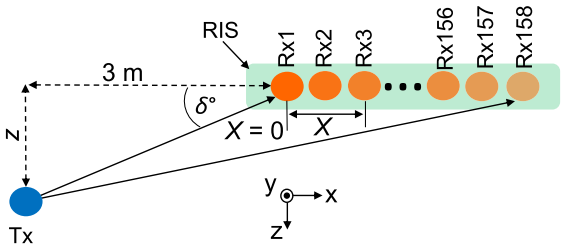

Fig. 4. Simulation setup of power received by RIS units. x (m) is the distance of a unit cell from the first cell (Rx1), and δ (°) is the incidence angle.

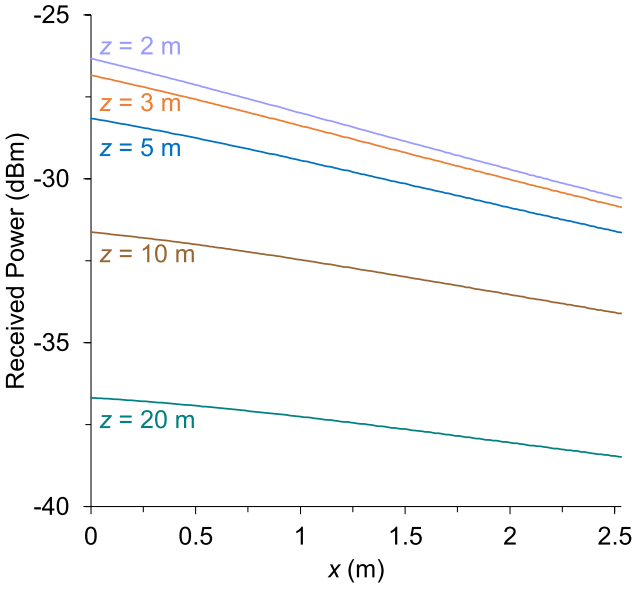

Fig. 5. Received power versus x plot. P_{rx} reduces with increasing x.

where P_{rx}, P_{in}, G_{tx}, G_{rx}, λ, θ, and r indicate received power (dBm), input power (18 dBm), transmitter gain (8 dBi), receiver gain (dBi), wavelength (0.143 m at 2.1 GHz), angle of incidence, and the distance between the transmitter and the receiver (m), respectively. The power received by each element is shown in Fig. 5 for varying levels of normal distance (z) between the Tx and the RIS. The angle of incidence of the

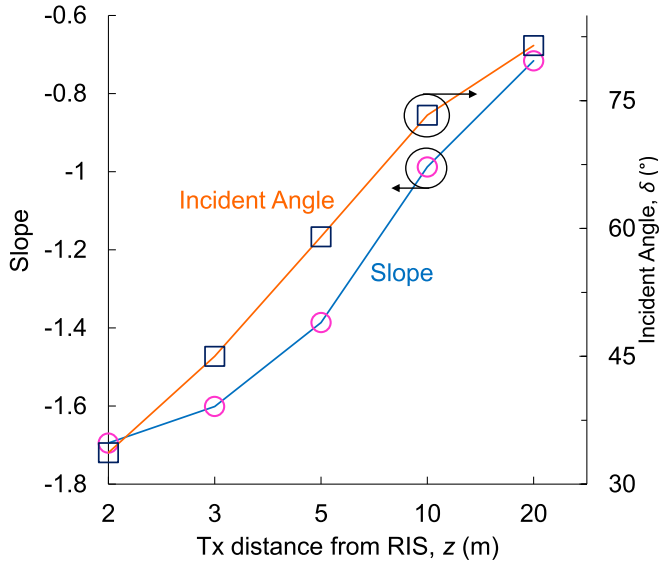

Fig. 6. Slope of the received power versus x and incident angle versus x curves.

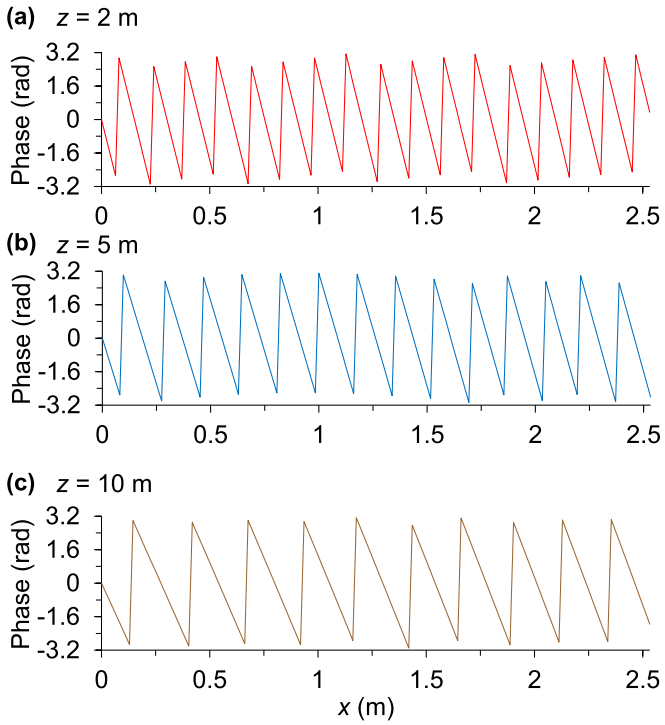

Fig. 7. Phase variation (normalized and wrapped) along the RIS unit cells when the distance between the transmitter and the RIS is (a) 2 m, (b) 5 m, and (c) 10 m.

transmitted radio wave changes with z. For a wide range of z values, we observe that there is always a gradient in the received power. In other words, the received power is high for unit cells closer to the Tx and low for distant cells. The slope of the received power versus x curve is plotted in Fig. 6. It is evident that the power distribution along the RIS is a function of the distance between the transmitter and the RIS. Fig. 7 shows the received signal phase variation for the receiver units.

2) Two-Dimensional Arrangement: We also simulated a 2-D RIS with eight rows and 158 columns (Fig. 9) in Wireless Insite [14]. Similar to the 1-D arrangement, the received power diminishes along the x-direction as the separation between the Tx and the unit dipoles increases (Fig. 10). The phase of the received signal demonstrates a periodic pattern along the x-axis (Fig. 11).

Prior knowledge of the received power phase distribution along the RIS unit cells can greatly benefit the state-selection procedure of RIS. The phase distribution is dependent on the direction of arrival (DoA) of the transmitter signal. Therefore, the fundamental proposition of our work is established. Later, we will show how the received RF power is converted to dc using different approaches through experimentation. Fig. 8 shows the block diagram for predicting the relative phase distribution across an RIS.

IV. Experimental Setup

A. Rectifier Design

The rectifier (Fig. 12) is fabricated on a 1.6-mm-thick FR4 substrate. A 50 Ω subminiature version A (SMA) connector connects the rectifier with the receiver antenna. The incoming RF signal passes through a matching network consisting of a series capacitor (C_2 = 100 pF) and a parallel inductor (L_2 = 2.2 nH). A Schottky diode (D, model: MA4E20541-1141T) in series converts the RF signal to dc. The rectified dc power is stored in the load capacitor (C_L) that is charged during the positive cycle and feeds the load resistor (R_L) during the negative cycle. An additional capacitor C_3 sits between C_2 and the Schottky diode D. A variable dc voltage source V_{dc} is placed across C_3. Two 220 nH inductors are used as RF chokes for blocking the RF signal from traveling into the dc circuit. The dc ground is connected to the RF ground through L_1. C_2 and C_3 block any dc component from flowing toward the RF source (or the receiver antenna). Fig. 2 shows the reflection coefficient (S_{11}) of the rectifier as a function of frequency. The rectifier is resonant at 2.1 GHz. Fig. 13 shows the rectifier output voltage versus input power (at the rectifier port) plot. The intrinsic sensitivity of the rectifier is −42 dBm. In other words, the rectifier can detect radio waves stronger than −42 dBm.

Due to the nonlinear nature of diodes, the rectifier also demonstrates nonlinearity in Fig. 13. For a given rectifier–RIS combination, the input RF power can be obtained from a lookup table (Fig. 13) saved in the controller unit. Fig. 14 shows the fabricated prototype of the RIS along with the rectifier. A coaxial cable (with SMA connectors) connects the unit dipole and the rectifier.

B. RF Energy Harvesting

The effectiveness of the proposed system is strongly dependent on the sensitivity of the energy harvesting circuit (rectifier). We propose four methods (Fig. 15) of received power rectification.

1) Direct Rectification: The power received by the RIS unit pair dipole is directly fed to the rectifier circuit and converted to dc. While this is the simplest approach, the sensitivity of the system is low and the effective range is the lowest of the considered techniques.

2) Rectification With DC Bias: The power required to activate the Schottky diode is the limiting factor in the RF–dc conversion. If the input RF power level is insufficient for diode activation, it is possible to bias the diode by inserting

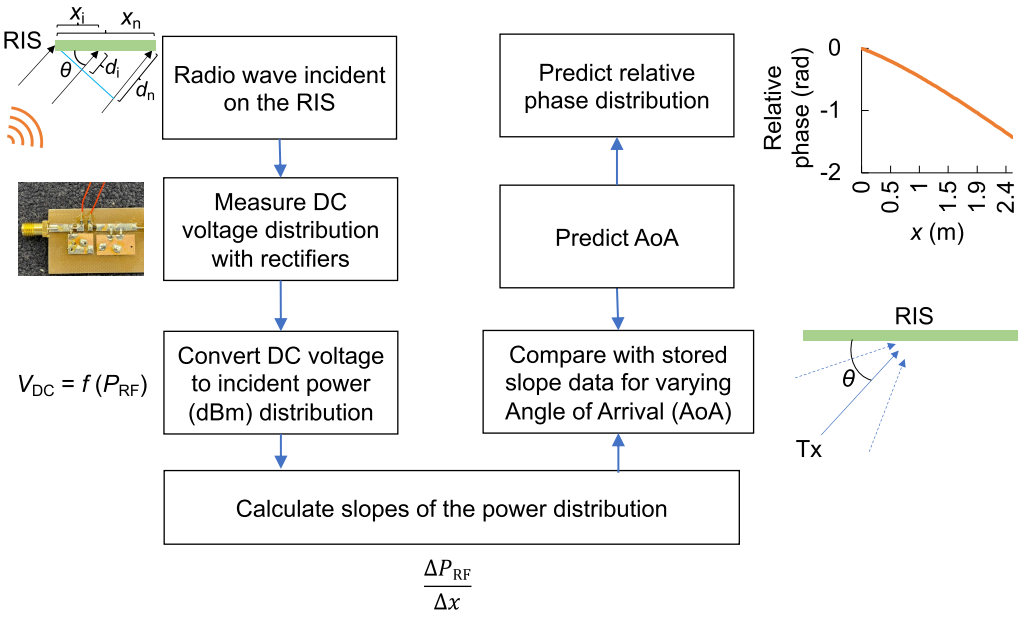

Fig. 8. Flowchart for predicting relative phase distribution.

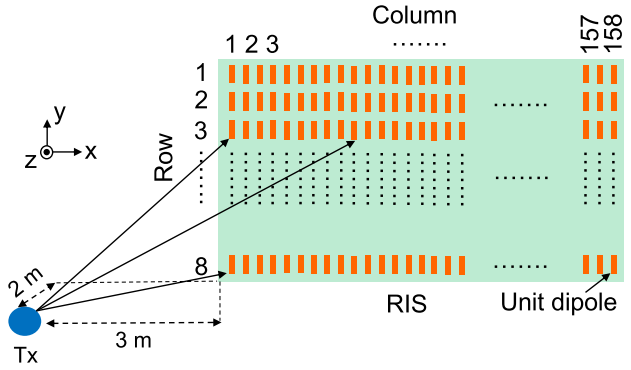

Fig. 9. Simulation setup of the 2-D RIS with a dipole transmitter.

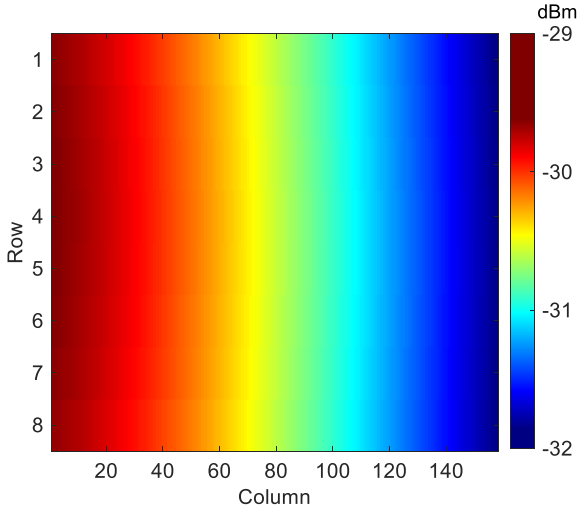

Fig. 10. Received power in a 2-D RIS (8 × 158).

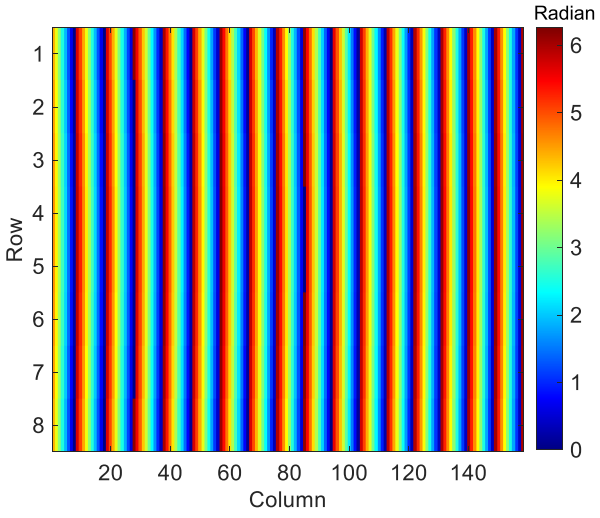

Fig. 11. Phase distribution in a 2-D RIS (8 × 158).

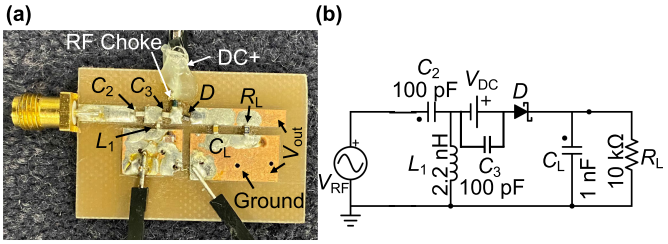

Fig. 12. (a) PCB prototype and (b) circuit representation of the rectifier.

a small amount of dc voltage (12.7 mV in our experiment) in the rectifier circuit. The effective range is higher than direct rectification. For identical reception scenarios, the rectifier output level will be higher with dc bias compared to direct rectification, reducing the burden on the sensitivity of the controller (typically microcontrollers).

3) Rectification With RF Amplifier: The sensitivity of the system can also be enhanced by introducing an RF amplifier in between the RIS unit cell diode and the rectifier. The availability of RF amplifiers in subminiature packages makes it a practical solution for extending the range of the proposed system. We used a 15 dB RF amplifier for our experiments.

4) Rectification With RF Amplifier and DC Bias: The simultaneous inclusion of RF amplifiers and dc bias provides a

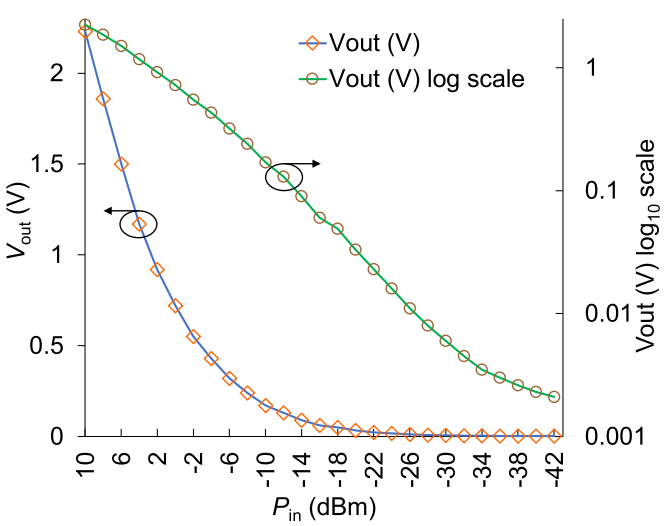

Fig. 13. Harvested dc output voltage versus input power plot.

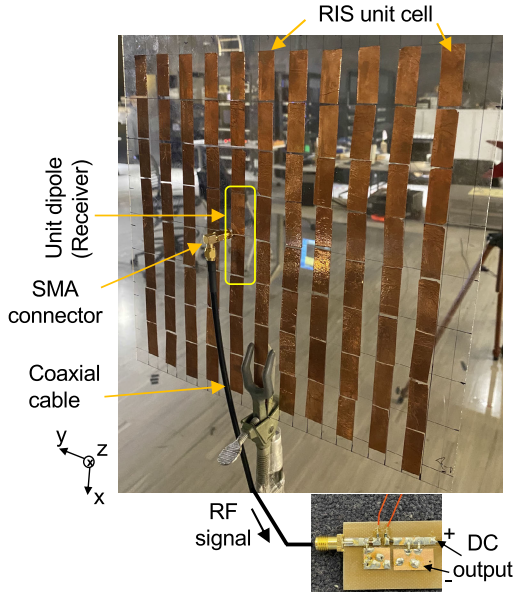

Fig. 14. Fabricated RIS prototype.

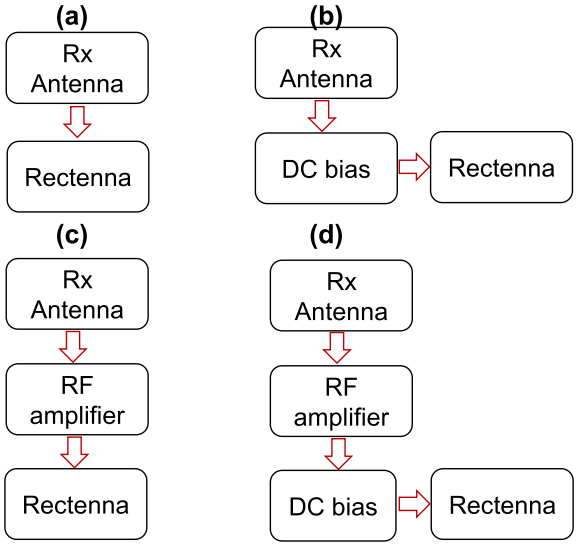

Fig. 15. Four proposed circuit arrangements. (a) Direct rectification. (b) Rectification with dc bias. (c) Amplification of the received signal using an RF amplifier. (d) Joint use of RF amplifier and dc bias.

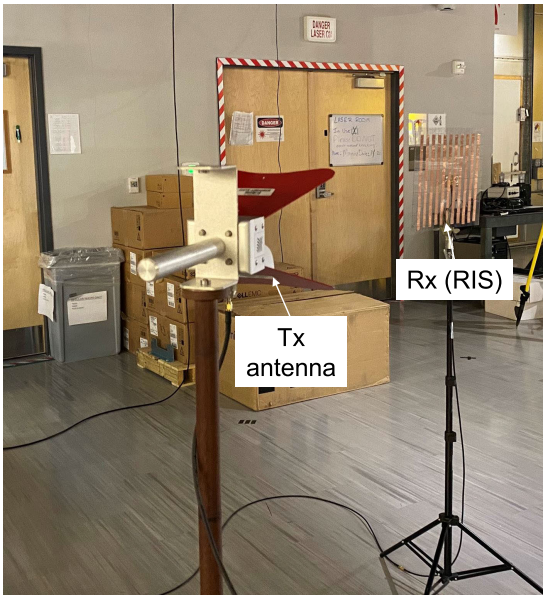

Fig. 16. Experimental setup.

maximum boost to the system's sensitivity. This arrangement provides the maximum effective range and the highest output voltage levels.

C. Experimental Setup

Figs. 16 and 17 show the experimental setup in a large indoor environment. A 2.1-GHz double-ridge horn antenna with a maximum gain of 8 dBi was used as the transmitter. The separation between the Tx and Rx was chosen to ensure that both antennas are in each other's far-field. The far-field distance of the transmitter (horn) antenna is greater than 0.33 m at 2.1 GHz. The minimum distance between the Tx and Rx (Tx2 and Rx1 pair) is larger than the far-field distance of the larger antenna (transmitter horn). Since most radio antennas in real life are omnidirectional, we always focused the transmitter horn toward the RIS (Rx). In other words, the transmitter was effectively an 8 dBi omnidirectional radiator.

An SMA connector connecting two unit cells form a diode that was used as the receiver. Both the transmitter and the receiver were used in vertical polarization, 1.2 m from the ground. The transmitter was placed in two different positions (Tx1 and Tx2), and the receiver was placed in three positions (Rx1, Rx2, and Rx3). An RF signal generator fed the transmitter with a constant 18 dBm power (continuous wave). The receiver (RIS unit cell diode) was connected to the rectifier through a coaxial cable. For each Tx–Rx pair, the received power was measured using a spectrum analyzer, and the rectified voltage level (at the rectifier output) was measured with a multimeter.

We conducted two rounds of experiments: 1) angular incidence: when the radio wave is incident at an acute angle with the center of the RIS and 2) normal incidence: when the radio wave is incident perpendicularly on the center of the RIS.

V. Results and Discussion

A. Energy Harvesting From RIS

Fig. 18 shows the rectified (harvested) voltage from the angular incidence of the radio waves on the RIS. The direct

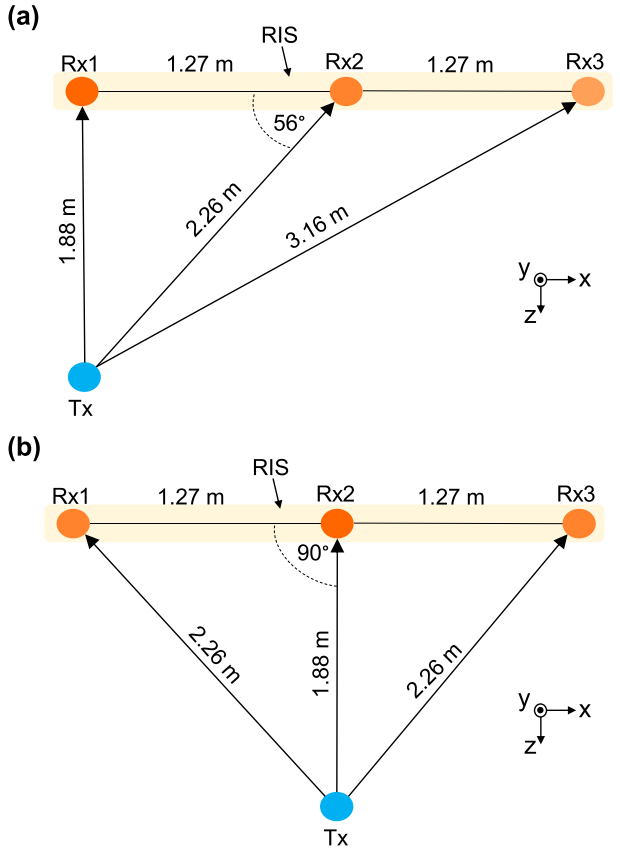

Fig. 17. (a) Angular incidence and (b) normal incidence of the radio wave.

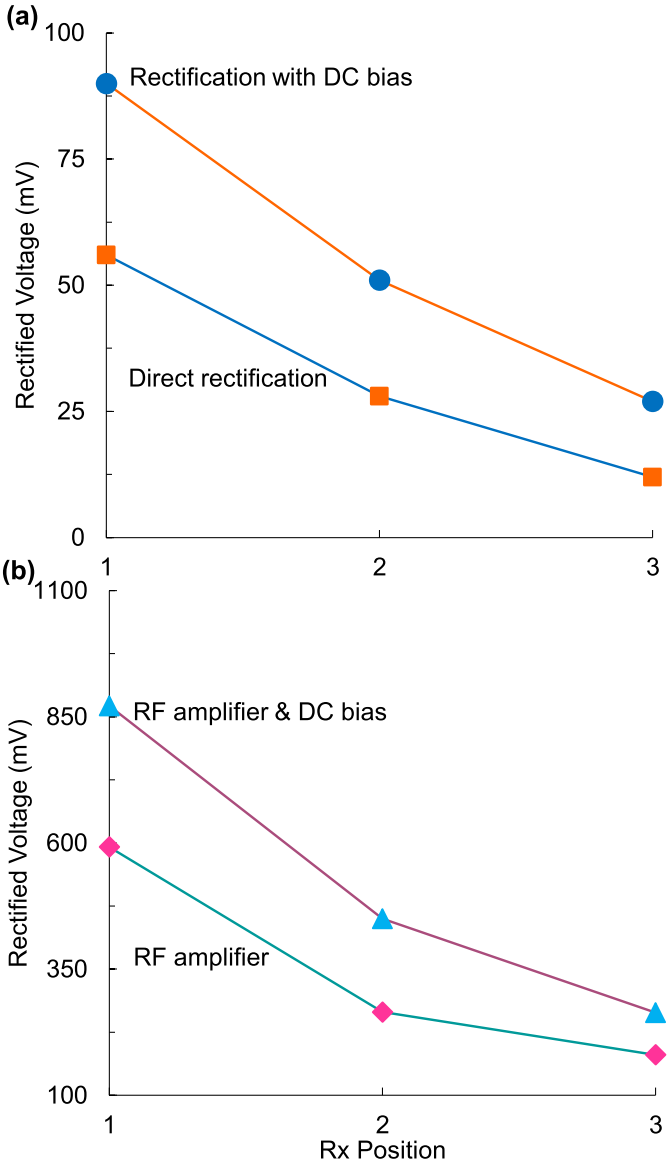

Fig. 18. Harvested DC output for angular incidence using (a) direct rectification, rectification with DC bias, (b) RF amplifier, and RF amplifier with DC bias.

rectification method yields minimum dc output. With the insertion of 12.7 mV dc bias voltage, the output voltage level is improved significantly (more than 12.7 mV). The improvement in dc output [Fig. 18(a)] with a small bias voltage is not uniform at the receiver positions due the nonlinearity of the Schottky diode. In other words, since the IV (current–voltage) curve of the Schottky diode is nonlinear, the current through the diode will depend on the input voltage. As a result, the current through the load varies with the input power level, resulting in different levels of improvement in the rectified voltage (based on receiver locations). The elevated output power level increases the range of the system and relaxes the restrictions (for scenarios identical to direct rectification) on the sensitivity of the dc detector on the controller side.

The RF amplifier (15 dB) improves the rectified voltage level more than ten times. The RF amplifier enhances the range of the proposed system by increasing the sensitivity. The RF amplifier and dc bias combination produce the maximum output. It is also clear that the dc insertion creates uneven improvement [Fig. 18(b)] in rectified voltage that is also seen in Fig. 18(a).

B. Power and Relative Phase Distribution

We are able to predict the power levels and the pattern of the power distribution (at the receiver locations) for both angular and normal incidences (Fig. 19). The rectified voltage outputs are mapped (predicted) into output power using Fig. 13. The RIS comprises of thousands of switchable unit dipoles. It would be infeasible to accommodate energy harvesting units for each unit. However, it would be possible to predict the overall power and relative phase distribution around the RIS by placing a limited number of energy harvesting units. The steps for predicting the relative phase distribution are explained as follows.

1) First, a radio wave hits the RIS.
2) The energy harvesting rectifiers distributed across the RIS convert the RF signal into dc.
3) The dc output of a rectifier is a function of the incident RF power level (Fig. 13). As a result, the dc voltage distribution can be converted to incident RF power (P_{RF}) distribution.
4) The slope is calculated at every point of the RF power distribution curve. Each Angle of Arrival (AoA, θ) leads to a unique slope distribution ($\Delta P_{\mathrm{RF}}/\Delta x$) across the RIS.
5) The slope distribution is then compared with stored slope data for varying AoAs.
6) The AoA associated with a slope distribution matches our calculated slope distribution. The AoA is accepted.

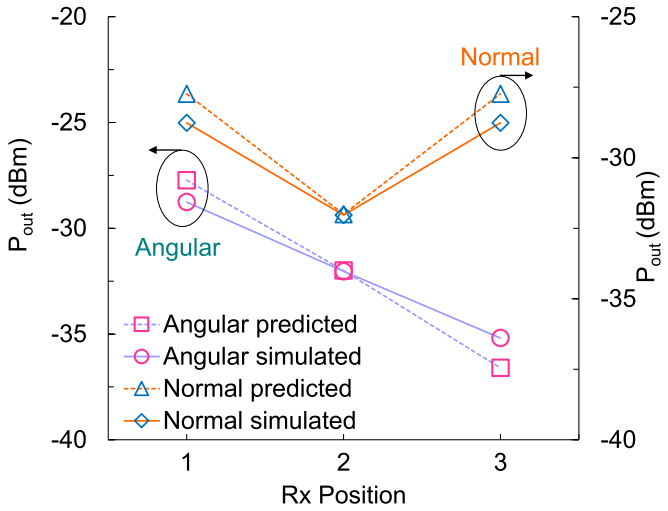

Fig. 19. Simulated and predicted (from V_{out}) received power by the RIS.

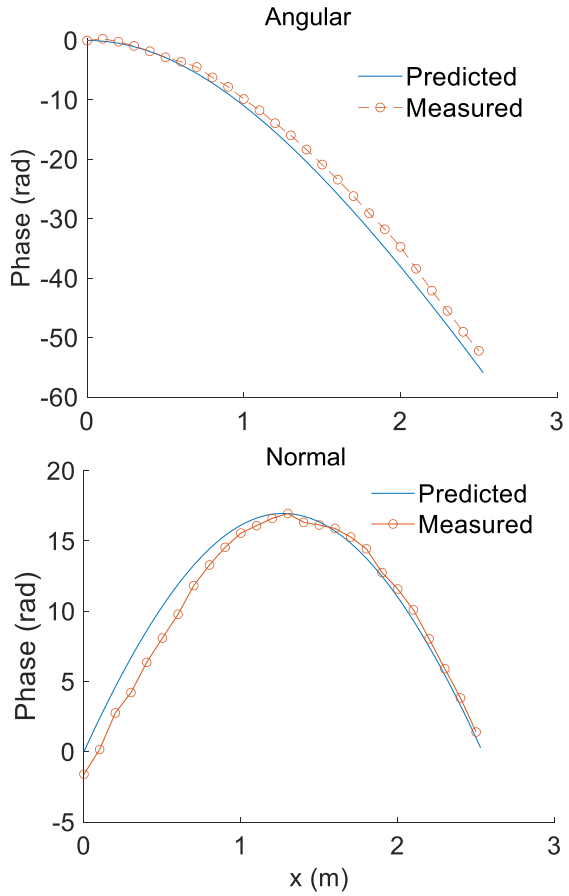

Fig. 20. Comparison between predicted and measured relative phase (normalized and unwrapped) distribution for (a) angular and (b) normal incidence.

7) The relative phase distribution is predicted based on the AoA. The incident wave travels varying distances to reach the RIS unit cells. Therefore, the incident wave hits different unit cells at different phases. If we calculate phase from the nearest peripheral unit cell ($\phi_1 = 0$ rad) from the transmitter side (cell-1 in this case), the additional path difference for the next elements can be calculated from the AoA. If θ is the AoA and the radio wave travels an additional d_i distance to reach the ith unit cell (x_i distance from cell-1) (Fig. 8), $d_i = x_i \cos(\theta)$. The relative phase (ϕ_i) of the incident RF wave at the ith element is

$$\phi_i = -\frac{2\pi}{\lambda} d_i = -\frac{2\pi}{\lambda} x_i \cos(\theta). \tag{3}$$

In other words, we can predict the relative phase distribution throughout the RIS. The overall relative phase distribution across the RIS would be $-(2\pi/\lambda)(x_1, x_2, x_3, \ldots, x_n)\cos\theta$, where n is the number of columns in the RIS.

Fig. 20 shows a comparison between the simulated and predicted relative phase distribution for angular and normal incidence (depicted in Fig. 17). In both cases, the phase distributions are normalized and unwrapped.

C. RIS State Selection

The proposed system can facilitate the existing RIS state-selection algorithms. A rectifier-assisted RIS state-selection algorithm can be developed using the following steps.

1) First, the radio signal is incident on the RIS.
2) Sparsely distributed rectifier circuits convert the incident radio energy into dc voltage (V_{out}) using any of the four proposed methods.
3) The RIS switch controller obtains the distribution of V_{out}. A V_{out} to P_{out} chart (similar to Fig. 13) is used to convert the dc voltage distribution to received RF power distribution.
4) At this step, the RIS unit dipoles are considered the elements of a 2-D array of antennas. The input power of each array element would be known by subtracting the Ohmic and dielectric loss in the antenna (can be considered uniform for all elements, except for peripheral elements) from the P_{out} values.
5) The RIS controller decides the switching combination to steer the reflected beam to the desired direction. The RIS state-selection problem is thus converted to a much simpler and more deterministic phased array switching problem.

Simulated and practical power and phase relations will not match accurately due to the dynamic nature of practical channels and the limitation of simulation. Therefore, a learning-based algorithm can be developed for the state-selection problem. Channel emulation [15] and transfer learning [16] can also be advantageous for a rapid state selection and a seamless integration of the RIS to the network.

The presence of multipath components will impact the power distribution in the RIS. Nevertheless, the energy harvesting circuit will still be able to detect the power distribution throughout the surface. In our experiment, we only considered one RIS, whereas, in a practical scenario, multiple RISs will work in conjunction. It has been shown that the multipath fading effect can be eliminated when all reflectors in the environment are coated with RIS [17], [18], [19].

VI. Conclusion

We established and demonstrated the applicability of energy harvesting rectifiers for estimating incident power and relative phase mapping across RISs. The proposed method can

potentially simplify and speed up the state-selection process for RIS. Using a combination of simulation and experimentation, we showed that the received power and relative phase distribution across an RIS can be predicted from the harvested energy levels. One of the limitations of the proposed method is the presence of nulls in the radiation pattern of the unit dipoles in the RIS. However, it is possible to acknowledge the impact of the null by incorporating ML algorithms. We have demonstrated incident power mapping in 1-D and 2-D RISs. In the future, we will demonstrate the implementation of the proposed technique in state-selection algorithms.

ACKNOWLEDGMENT

Any opinion, findings, and conclusion or recommendations expressed in this material are those of the author(s) and do not necessarily reflect the views of the National Science Foundation.

REFERENCES

[1] B. Clerckx, J. Kim, K. W. Choi, and D. I. Kim, "Foundations of wireless information and power transfer: Theory, prototypes, and experiments," *Proc. IEEE*, vol. 110, no. 1, pp. 8–30, Jan. 2022.

[2] V. Arun and H. Balakrishnan, "RFocus: Beamforming using thousands of passive antennas," in *Proc. 17th USENIX Symp. Netw. Syst. Design Implement. (NSDI)*, 2020, pp. 1047–1061.

[3] B. Sheen, J. Yang, X. Feng, and M. M. U. Chowdhury, "A digital twin for reconfigurable intelligent surface assisted wireless communication," 2020, *arXiv:2009.00454*.

[4] A. Taha, M. Alrabeiah, and A. Alkhateeb, "Deep learning for large intelligent surfaces in millimeter wave and massive MIMO systems," in *Proc. IEEE Global Commun. Conf. (GLOBECOM)*, Dec. 2019, pp. 1–6.

[5] B. G. Kashyap, P. C. Theofanopoulos, Y. Cui, and G. C. Trichopoulos, "Mitigating quantization lobes in mmWave low-bit reconfigurable reflective surfaces," *IEEE Open J. Antennas Propag.*, vol. 1, pp. 604–614, 2020.

[6] H. Kamoda, T. Iwasaki, J. Tsumochi, T. Kuki, and O. Hashimoto, "60-GHz electronically reconfigurable large reflectarray using single-bit phase shifters," *IEEE Trans. Antennas Propag.*, vol. 59, no. 7, pp. 2524–2531, Jul. 2011.

[7] X. Tan, Z. Sun, D. Koutsonikolas, and J. M. Jornet, "Enabling indoor mobile millimeter-wave networks based on smart reflect-arrays," in *Proc. IEEE INFOCOM Conf. Comput. Commun.*, Apr. 2018, pp. 270–278.

[8] W. Tang et al., "Programmable metasurface-based RF chain-free 8PSK wireless transmitter," *Electron. Lett.*, vol. 55, no. 7, pp. 417–420, Apr. 2019.

[9] T. J. Cui, M. Q. Qi, X. Wan, J. Zhao, and Q. Cheng, "Coding metamaterials, digital metamaterials and programmable metamaterials," *Light, Sci. Appl.*, vol. 3, no. 10, p. e218, Oct. 2014.

[10] X. Wan, M. Q. Qi, T. Y. Chen, and T. J. Cui, "Field-programmable beam reconfiguring based on digitally-controlled coding metasurface," *Sci. Rep.*, vol. 6, no. 1, pp. 1–8, Feb. 2016.

[11] X. Pei et al., "RIS-aided wireless communications: Prototyping, adaptive beamforming, and indoor/outdoor field trials," *IEEE Trans. Commun.*, vol. 69, no. 12, pp. 8627–8640, Dec. 2021.

[12] C. Huang, G. C. Alexandropoulos, C. Yuen, and M. Debbah, "Indoor signal focusing with deep learning designed reconfigurable intelligent surfaces," in *Proc. IEEE 20th Int. Workshop Signal Process. Adv. Wireless Commun. (SPAWC)*, Jul. 2019, pp. 1–5.

[13] C. Liaskos, A. Tsioliaridou, S. Nie, A. Pitsillides, S. Ioannidis, and I. Akyildiz, "An interpretable neural network for configuring programmable wireless environments," in *Proc. IEEE 20th Int. Workshop Signal Process. Adv. Wireless Commun. (SPAWC)*, Jul. 2019, pp. 1–5.

[14] *Wireless InSite*. Accessed: May 12, 2022. [Online]. Available: www.remcom.com/wireless-insite-em-propagation-software

[15] M. A. S. Tajin, M. Jacovic, G. Dion, W. M. Mongan, and K. R. Dandekar, "UHF RFID channel emulation testbed for wireless IoT systems," *IEEE Access*, vol. 9, pp. 68523–68534, 2021.

[16] C. T. Nguyen et al., "Transfer learning for future wireless networks: A comprehensive survey," 2021, *arXiv:2102.07572*.

[17] R. Zhou et al., "Modeling and measurements for multi-path mitigation with reconfigurable intelligent surfaces," in *Proc. 16th Eur. Conf. Antennas Propag. (EuCAP)*, Mar. 2022, pp. 1–5.

[18] G. Wu, F. Li, and H. Jiang, "Analysis of multipath fading and Doppler effect with multiple reconfigurable intelligent surfaces in mobile wireless networks," *Wireless Commun. Mobile Comput.*, vol. 2022, pp. 1–15, Jan. 2022.

[19] E. Basar, "Reconfigurable intelligent surfaces for Doppler effect and multipath fading mitigation," *Frontiers Commun. Netw.*, p. 672857, May 2021

Md Abu Saleh Tajin (Student Member, IEEE) received the B.S. degree in electrical and electronic engineering (EEE) from the Bangladesh University of Engineering and Technology, Dhaka, Bangladesh, in 2015, and the M.S. degree in electrical engineering from Drexel University, Philadelphia, PA, USA, in 2021, where he is currently pursuing the Ph.D. degree in electrical and computer engineering.

He was a member of the Drexel Wireless Systems Laboratory (DWSL). He was a Junior System Engineer at Bangla Phone Ltd., Dhaka, from 2015 to 2017. His research interests include wireless sensors, RF systems, 5G/6G, and the Internet of Things (IoT).

Kyei Anim received the B.Sc. degree in telecommunication engineering from the Kwame Nkrumah University of Science and Technology, Kumasi, Ghana, in 2014, and the M.Sc. and Ph.D. degrees in electronic engineering from Hanbat National University, Daejeon, South Korea, in 2017 and 2021, respectively.

He was with the Microwave and Antenna Laboratory, Hanbat National University, as a Post-Doctoral Researcher. He is currently a Post-Doctoral Research Fellow with the Drexel Wireless Systems Laboratory, Department of Electrical and Computer Engineering, Drexel University, Philadelphia, PA, USA. His research interests include mmWave reconfigurable antenna, wearable antennas and electronic devices, mmWave linear and high-gain and high-efficiency phased array for 5G, Wi-Fi, and satellite and radar applications.

Kapil R. Dandekar (Senior Member, IEEE) received the B.S. degree in electrical engineering from the University of Virginia, Charlottesville, VA, USA, in 1997, and the M.S. and Ph.D. degrees in electrical and computer engineering from The University of Texas at Austin, Austin, TX, USA, in 1998 and 2001, respectively.

In 1992, he was with the U.S. Naval Observatory, and from 1993 to 1997, he was with the U.S. Naval Research Laboratory. In 2001, he joined the Electrical and Computer Engineering Department, Drexel University, Philadelphia, PA, USA, where he is currently the E. Warren Colehower Chair Professor in electrical and computer engineering and the Director of the Drexel Wireless Systems Laboratory (DWSL). He is an Associate Dean with the Enrolment Management and Graduate Education, Drexel University College of Engineering. DWSL has been supported by the U.S. National Science Foundation, National Institutes of Health, DARPA, Army CERDEC, National Security Agency, Office of Naval Research, and Private Industry. His current research interests and publications involve wireless communications, software-defined radio, reconfigurable antennas, and smart textiles. Intellectual property from DWSL has been licensed by external companies for commercialization.

Dr. Dandekar was also a member of the IEEE Educational Activities Board. He is the Co-Founder of the EPICS-in-IEEE Program.